

Prognosis of Li-ion batteries under large load variations using hybrid physics-informed neural networks

Kajetan Fricke¹, and Renato G. Nascimento², and Matteo Corbetta³, and Chetan S. Kulkarni⁴, and Felipe A. C. Viana⁵

^{1,2,5} *Department of Mechanical and Aerospace Engineering, University of Central Florida, Orlando, FL, 32816, USA*
kajetanfricke@knights.ucf.edu
renato.gn@knights.ucf.edu
viana@ucf.edu

^{3,4} *KBR, Inc., NASA Ames Research Center, Moffett Field 94035 CA, USA*
matteo.corbetta@nasa.gov
chetan.s.kulkarni@nasa.gov

ABSTRACT

The development of new modes of transportation such as electric vertical takeoff and landing aircraft and the use of drones for package and medical delivery have increased the demand for reliable batteries. Capacity degradation and discharge behavior can vary from battery to battery and can also be influenced by changes in load due to internal thermal stress. Therefore, predicting the degradation of a battery's state-of-health (SOH) and state-of-charge (SOC) is a crucial task to ensure high reliability standards and prevent failures during operation. At the same time, recent advanced in physics-informed machine learning models have demonstrated potential to model both SOC and SOH, merging physics-derived equations and data-driven kernels in a hybrid model trained with back-propagation.

In this paper, we enhance a hybrid physics-informed machine learning version of a Li-ion battery model we presented in previous works. The enhanced model captures the effect of wide variation of load levels, in the form of input current, which causes large thermal stress cycles. The cell temperature build-up during a discharge cycle is used to identify temperature-sensitive model parameters. We also extend the aging model built upon cumulative energy drawn by introducing the effect of load levels. We then map cumulative energy and load level to battery capacity with Gaussian process regression.

To validate our approach we use a battery aging dataset collected on a self-developed testbed, where we used a wide current level range to age battery packs in an accelerated fashion. Prediction results show that our model can be successfully calibrated and generalizes across all applied load levels.

Kajetan Fricke et al. This is an open-access article distributed under the terms of the Creative Commons Attribution 3.0 United States License, which permits unrestricted use, distribution, and reproduction in any medium, provided the original author and source are credited.

1. INTRODUCTION

The market for electric drive train powered vehicles such as electric cars and, in the near future, eVTOL drones is growing with noticeable speed. One main cost driver of electric vehicles is hereby the battery pack, contributing up to 40% to the overall vehicle cost (Lutsey & Nicholas, 2019). Reliable prediction methods for battery state of charge and health could enable usage optimization for operators of electric powered vehicle fleets, and be crucial for safe and reliable operation. Electrochemistry-based models can accurately predict SOC and SOH with adequate precision, but can be computationally expensive and, therefore, suitable for in-time monitoring only to a limited extend. Furthermore, large variations in operating conditions impose a challenging framework for high-fidelity electrochemistry-based models, due to the main challenges of model parameter optimization, which is usually performed for a specific operating point and might lead to sub-optimum predictions further away from the primary design point. Reduced order models, on the other hand, can be suitable for online prediction due to low computational cost. They are recognized as a powerful tool in prognostics applications for industrial equipment, at the cost of some accuracy loss.

The use of purely data-driven approaches for surrogate modeling requires a constant tracking of the input-output relation through sensors or indirect estimates which, in many engineering applications, is not feasible nor economically beneficial. Critical useful data are usually scarce, thus invalidating one of the key requirements of traditional machine learning models.

In order to mitigate the drawbacks of the aforementioned approaches, in this paper, we present an enhanced version of a hybrid modeling approach for state of charge and health prediction of lithium ion batteries. Our approach builds on top of a combined electrochemistry based battery SOC and SOH model, which was initially introduced by (Daigle & Kulkarni,

2013), with a data-driven approach presented in (Nascimento, Corbetta, Kulkarni, & Viana, 2021a). This hybrid physics-informed machine learning approach implements reduced order models based on the Nernst and Butler-Volmer equations and utilizes a data-driven layer to reduce the remaining discrepancy between actual and predicted battery voltage during discharge. It is placed within an recurrent neural network (RNN) cell in order to predict the voltage on a discharge time series. This model approach proved its prediction capabilities on low level discharge loads up to 4 A (Nascimento, Corbetta, Kulkarni, & Viana, 2021b), (Bole, Kulkarni, & Daigle, 2014).

In order to predict the SOC for batteries subjected to a wide range of load levels, as real-world applications will require, we improve the hybrid approach by adapting both the data-driven and electrochemistry based model portions to capture a large variety of load levels and the effect of temperature build-up during discharge caused by such load variations. Furthermore, we aim to forecast battery aging through the prediction of model parameters correlated with the battery residual capacity, which we describe informally as aging parameters. We use Gaussian process models to predict such aging parameters as function of cumulative energy and discharge load levels. With the cost associated to real world data acquisition in mind, we build the models in order to be able to predict battery discharge and degradation with only few early life data points, and degradation information gathered from a fleet of similar batteries subjected to different load levels.

The dataset used in this research is extracted from battery life cycle tests carried out at the Probabilistic Mechanics Laboratory at the University of Central Florida, using a self-developed battery life cycle test bed. Results show that the extension of our hybrid battery model can help to improve predictions of SOC on wide load level ranges for both constant and variable loading conditions. Battery aging resulting from usage and affected by load level variations can be captured by the hybrid model and could potentially help operators to track the state of health of batteries operated in large fleets. Our model is implemented using Python, applying the deep learning package Pytorch (Paszke et al., 2019) and the Gaussian process package GPyTorch (Gardner, Pleiss, Bindel, Weinberger, & Wilson, 2018).

The remaining of this paper is organized as follows. Section 2 offers a brief literature review and Section 3 presents the battery life cycle dataset used in this research. Section 4 introduces the improved hybrid model approach and Section 5 outlines the model used for aging prediction and highlights the achieved SOC prediction results. Section 6 offers a brief summary and discusses potential future work.

2. BACKGROUND AND LITERATURE REVIEW

This section provides a short overview of the existing literature on battery SOC and SOH prognosis, where we want

to highlight key studies and different modeling approaches that provide necessary context for our own work. Here, we divide these modeling approaches in two groups: 1) purely electrochemistry and first principle-based models, purely data-driven, and 2) hybrid modeling approaches that combine both aforementioned techniques.

Recent works in the field of data-driven models include the contribution of (Zhang, Xiong, He, & Liu, 2017), where authors employ a long short-term memory (LSTM) cell within a RNN for battery remaining useful life prediction. Battery cell capacity degradation data is used to train the LSTM cell parameters until a certain life threshold; the model is then used to predict capacity degradation until reaching end-of-life (EOL). The optimization of model parameters is performed using the RMSprop. Tampier and collaborators (Tampier Cotoras et al., 2015) compare particle filter and unscented Kalman filter algorithms both fused with feedback correction loops for SOC estimation and end-of-discharge (EOD) prediction. Authors identified advantages of a particle filter based estimation when deployed on a battery system model that lacks precision and further findings suggest better SOC prediction capabilities for the unscented Kalman filter in combination with a feedback loop if applied on a high fidelity model.

As an example of first principle-based models, Dubarry and collaborators (Dubarry, Truchot, & Liaw, 2012) presented a mechanistic model for battery prognosis. The synthetic approach models the specific electrode behavior and cell degradation in between both electrodes as a function of loading ratio. The model can distinguish between different cell aging processes depending on various degradation modes and can predict cell performance and degradation taking into account operating conditions and cell design. One main advantage of this approach is the flexibility regarding model adjustment for deployment on different battery chemistries, cell sizes and geometries, as well as aging conditions.

A hybrid model for battery SOH estimation was proposed by (Lyu, Wang, & Gao, 2021), where a multi-kernel relevance vector machine is trained to map battery aging features to capacity which was obtained through quantitative evaluations. The aging features are then decomposed in signals of different frequencies and modeled through a LSTM or feedforward neural network. Using the aforementioned neural network models, the battery SOH can be estimated online and EOL can be forecasted from the obtained aging feature predictions.

3. DATA

In this work we use a battery life cycle dataset collected on a self-developed battery test bed. The test bed provides continuous battery cycle capabilities for up to 6 batteries with acquisition of current, voltage and cell temperature throughout the entire cycle process. The batteries used in this research are composed of two 18650 Li-ion cells assembled in series (2S)

with a battery pack voltage ranging from 8.4 V to 5.0 V cut-off voltage. For life cycle testing, the batteries were divided in two different groups. One group was subject to constant load levels during discharge and the second group was discharged at variable loads. The constant current levels are 9.3 A, 12.9 A, 14.3 A, 16.0 A and 19.0 A, whereas the two variable load levels ranged from 12.9 A-16.0 A and 16.0 A-19.0 A, in order to keep the discharge current within the maximum current rating of 20 A (“Introduction of INR18650-25R”, 2013). Two battery packs were cycled for each load condition, for a total of 14 batteries.

In order to determine battery capacity degradation during the life cycle process, after completing intervals of 20 high load discharge cycles, each of the batteries were discharged at a constant current level of 2.5 A, which is equivalent to the rated capacity of 2.5 Ah (1C). This slow-paced, constant load discharge ensures precise battery capacity estimate due to low temperature build-up and small Li-ion concentration gradients in the electrolyte of the positive and negative electrode. All batteries were subject to identical charging and resting procedures, with a charging current of 3 A during the constant current charging phase and resting phases of 10 A between each charging and discharge cycle. The battery aging procedure was carried out until reaching end of life (EOL), which corresponds to the failure of at least one of the two battery cells that make up a pack.

Figure 1 shows a constant and variable load discharge cycle each, chosen from the dataset, where the current levels applied to the battery is shown on the top and the corresponding battery voltage on the bottom plot. The variable load levels consist of missions with random portions of constant current applied for an interval within a 40-80 seconds range and with direct step input current switches to the following current level. The voltage discharge curve shows an instant initial drop from the fully charged voltage due to the applied high load levels. After a linear discharge trend the battery voltage then drops sharply right before reaching EOD at 5 V.

4. HYBRID PHYSICS-INFORMED NEURAL NETWORKS MODEL FOR BATTERY PROGNOSIS

In this research work, the electrochemistry based battery model presented by (Daigle & Kulkarni, 2013) serves as a baseline. Our goal is to enhance an extended approach of a hybrid model presented in (Nascimento, Fricke, & Viana, 2020) that incorporates two trainable parameters and two data-driven components. The trainable parameters are correlated with battery aging and will be discussed in more detail later in this section. Two multi-layer perceptrons (MLP) serve as data-driven components of our model, and are used to estimate the non-ideal voltage on the positive and negative electrode.

In order to simulate the state transformation at each step of the time series, we leverage the similarity between recurrent

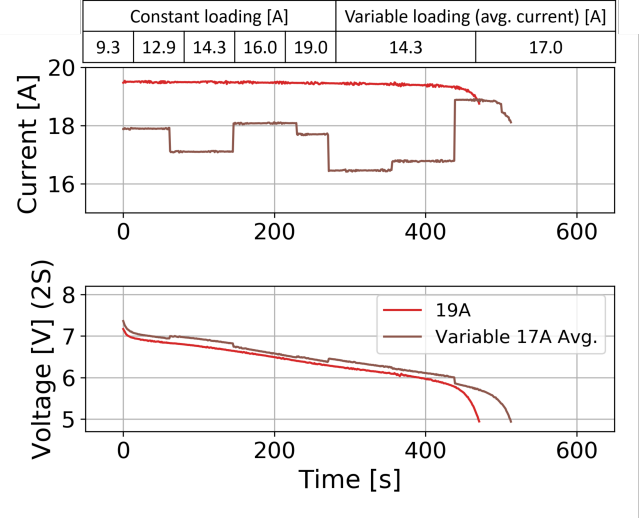


Figure 1. Examples of constant (red) and variable (brown) loading discharge cycles extracted from the accelerated battery life cycle dataset and a summary of the applied load levels (table on top).

neural networks (RNN) and Euler’s forward integration to model the time dependent response of the system. Using the input and previous state a RNN cell computes the current state (which then becomes the previous state for the next time step), and estimates the output at the current time step. Equation (4) defines the state transformation performed through the RNN cell, where t is time, y is the cell output, h is the internal state and u is the input to the RNN cell.

$$[y_t, \mathbf{h}_t]^T = \mathbf{f}(u_t, y_{t-1}, \mathbf{h}_{t-1}).$$

The internal state vector contains the ohmic and surface overpotentials as well as the available Lithium-ions on each electrode divided in bulk and surface volume. The applied current and cell temperature are model inputs, while voltage is the model output:

$$\mathbf{h} = [V_0, V_{\eta,n}, V_{\eta,p}, q_{b,n}, q_{b,p}, q_{s,n}, q_{s,p}]^T, \\ \mathbf{u} = [i, T], \quad \text{and} \quad \mathbf{y} = y = V.$$

The RNN cell design is presented in Fig. 2, where we combine the reduced-order electrochemistry based model portions (blue blocks) with a data-driven portion (green block), that are used to reduce the prediction error between model predictions and observed data, and aging parameters (yellow block) that are set as trainable parameters and intend to capture aging effects. Under ideal conditions the equilibrium potential on each electrode is estimated through the Nernst equation as described in (Daigle & Kulkarni, 2013), and the voltage drop due to the surface overpotential is estimated through the Butler-Volmer

model. Furthermore, the rate of change of the lithium-ion concentrations on the electrode surface and bulk volumes is estimated based on electrochemistry principles as function of the diffusion rate. For a more detailed description of the reduced order electrochemistry based equations, the interested reader is referred to Appendix A.

In order to compensate for the prediction error remaining after estimating the voltage by adding the equilibrium potential, surface overpotential V_η and ohmic overpotential V_o , two non-ideal voltage multi-layer perceptrons are implemented to estimate the internal voltage on the positive and negative electrode:

$$V_{ni,p} = \text{MLP}_p(x_p, i; \mathbf{w}_p, \mathbf{b}_p) \quad .$$

The MLP on the positive side receives the mole fraction x_p and the discharge current i as input in order to capture discharge effects resulting from a wide load level range. Neuron weights and biases are collected in vectors \mathbf{w}_p and \mathbf{b}_p . This MLP is build with two hidden layers with 8 neurons in the first layer and 4 in the second. The activation for both hidden layers is the hyperbolic tangent. The non-ideal voltage MLP for the negative side consists of only one neuron with linear activation function, since empirical analysis suggest a linear relation between the mole fraction x_n and V_{int} , and therefore only the mole fraction is used as input:

$$V_{ni,n} = \text{MLP}_n(x_n; \mathbf{w}_n, \mathbf{b}_n) \quad .$$

The battery aging parameters in this model are represented through the maximum number of available ions q^{max} as well as the base internal resistance at reference temperature R_b . Those parameters are trainable in order to capture the aging effects of the batteries during life cycling. Before starting the aging process, the battery cells used in this research have a total of $1.5 \cdot 10^4 C$ available ions, which decreases over time as discussed later in Section 5.2. In our model we implemented the change of internal resistance not only as function of aging, but also within a single discharge cycle due to temperature build-up, using Arrhenius' law:

$$R_o = R_b \cdot e^{R_\tau \left(\frac{1}{T} - \frac{1}{T_{ref}} \right)} \quad ,$$

where R_b represents the base resistance value that increases during aging but remains constant within a discharge cycle. Value R_τ drives the temperature-dependent change of internal resistance. T is the cell temperature measured in Kelvin and T_{ref} the reference temperature in Kelvin, which is commonly defined as ambient air temperature of 293 K. We set the initial value of the base internal resistance R_b to 30 m Ω , as per Samsung INR18650-25R datasheet. Parameter R_τ is tuned on initial discharge curves for all load levels in order to comply with the physical law of decreasing resistance due to temperature increase. Both internal resistance parameters are trained

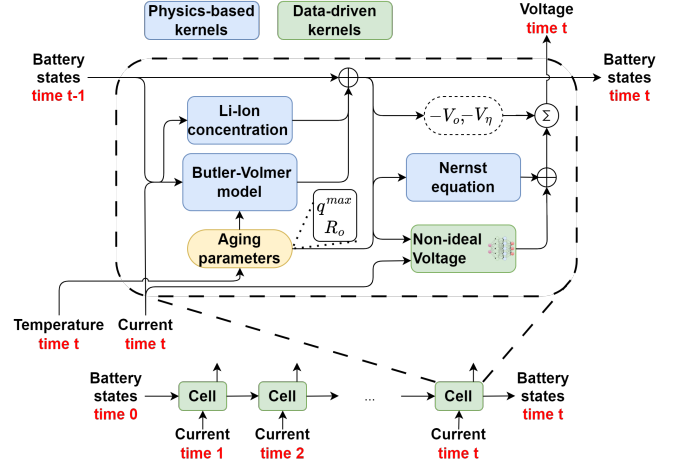


Figure 2. Physics-informed RNN cell incorporating electrochemistry baseline model and data-driven modeling of non-ideal voltage.

on early life discharge curves to characterize battery-to-battery variations. We used the same Arrhenius' law to model the effect of temperature on the diffusion constant, as shown in the Appendix. Since the battery packs used in this research consist of two cells connected in series (2S), we utilize the assumption the output voltage of the entire pack can be obtained through adding up the voltages of the cells connected in series.

5. LOAD LEVEL-DEPENDENT APPROACH TO DEGRADATION MODELING

5.1. Model Training on Constant Current Discharge

In order to train the hybrid physics-informed model, we first selected the constant-loading discharge curves from the life cycle data. This subset of the whole dataset consists of five load levels ranging from 9.3A to 19.0A, with two batteries cycled at each level. Figure 3 shows the training data selected from the four initial discharge cycles at each load level. The upper graph of the plot shows the measured voltage discharge curves from fully charged to maximum depletion at 5 V cut-off voltage. Each load level shows an initial voltage drop right after the load is applied, which turns out to be larger the more aggressive the loading conditions are. The main portion of the discharge curve follows a linear trend until a sharp drop right before reaching the cut-off voltage. As expected, the EOD time is reached earlier for more aggressive load levels.

The model training consists of: (i) initialization of the non-ideal voltage MLP parameters, using an approximate solution for the non-ideal voltage output, and (ii) the actual training of the MLPs on the early life training dataset on the discharge curves while keeping the aging parameters at their initial values. From our observations, we believe the non-ideal voltage relation to current and mole fraction remains approximately

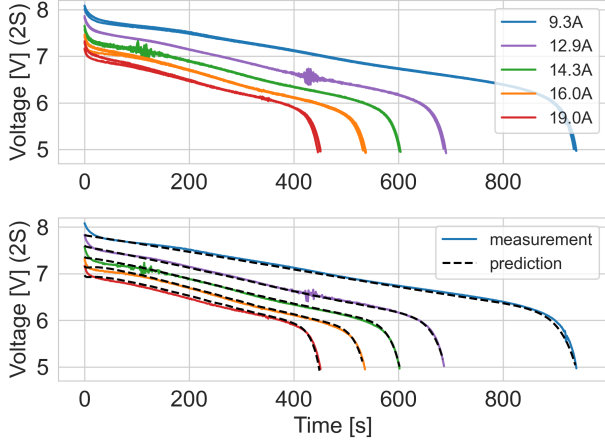


Figure 3. Constant current training data with wide load level range from 9.3 A to 19 A (top). Model predictions on training data plotted as dashed curves (bottom).

constant throughout the aging process, and therefore, the non-ideal voltage MLP weights and biases are frozen after being trained on early-life data. The next step consists of aging parameters (q^{max} , R_b) training on the early life (4 initial cycles) discharge curves for each constant load level, while keeping the trained MLP parameters frozen. This allows us to identify aleatory uncertainty on the aging parameters within the battery fleet, as load level variations show their effect later on in the battery life cycle but are negligible in the beginning.

After the model is trained on the early life training dataset, we performed predictions on the training data to assess the performance of the trained model. The dashed curves in the bottom subplot of Fig. 3 show the model predictions on top of the ground truth data, showing good agreement between the two. For quantitative performance validation, we use the root mean squared error (RMSE) over the entire discharge curve, as it is also used as metric in the loss function. Averaged for all load levels, the RMSE is $2.19 \cdot 10^{-2}$ V.

As important metric for model performance assessment is the EOD time, defined as the time necessary to reach a minimum voltage of 5.4 V. This limit was determined by including a reasonable safety margin over the actual battery EOD happening at the cut-off value of 5 V. This metric determines whether a model properly predicts the remaining usage time of a battery until reaching the end of safe battery operation. Figure 4 shows the predicted EOD over actual EOD for the 5 different constant-current load levels included in the training dataset. The EOD time covers a wide range from roughly 450 seconds (19 A discharge) to above 900 seconds (9.3 A discharge), where four different EOD time predictions for each load level are plotted. It can be observed that the predictions of EOD align closely with the actual EOD for all load levels, as all points fall within a 3% error band. The RMSE for EOD

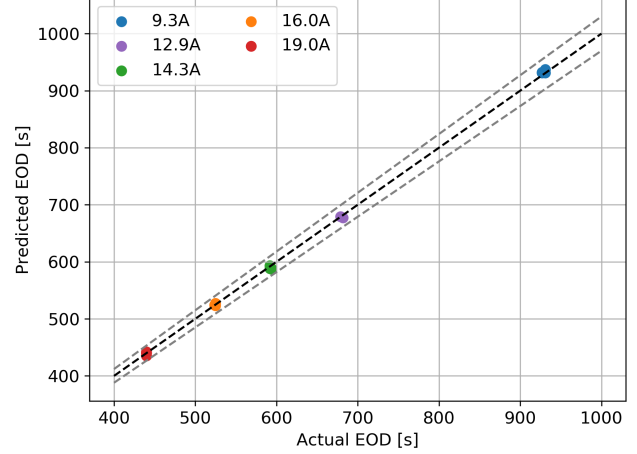


Figure 4. End-of-discharge: Prediction against actual EOD for constant current training data. The dashed lines represent a +/- 3% error band.

time is 3.7 s with a discharge time range of 450-900 seconds.

In order to validate the performance of the discharge prediction model, variable loading curves that are not used in the training dataset serve as validation dataset. Figure 5 shows the variable load discharge curves for the range 16 A - 19 A in the top row and for 12.9 A - 16 A in the bottom row. The solid gray lines represent the measured discharge curve, whereas the dashed lines show the model prediction. Two different discharge curves for each battery are shown in the plot. Predictions on the aggressive load profile in the top row follow the linear discharge trend fairly well and also capture the EOD quite accurately within a 1% error interval. Some predictions on battery 2 struggles to replicate the staircase-like discharge behavior resulting from the variable loading conditions. The predictions for the batteries subject to less aggressive variable discharge profiles, shown in the bottom row, accurately follow the linear discharge trend and predict EOD also within a 1% error interval. Here, the model shows a quite precise prediction alignment with the actual data, where only minor deviations (e.g. battery 4) from the staircase-like voltage curves are observed. Assessing the prediction results quantitatively shows that the RMSE remains within 1.08×10^{-1} V for all presented battery predictions, which means an RMSE of less than 2% of the ground truth voltage.

Once the non-ideal voltage MLP and the aging parameters have been trained on early life curves across all load levels, predictions on later life stages can be performed to determine model performance on aged batteries without updating the model parameters. By so doing, model parameters that require adjustment due to aging effects can be identified. Figure 6 shows the discharge curve prediction for one of the batteries subjected to variable load between 12.9 A and 16 A, early in life (left column) and with increasing age in 20 cycle intervals,

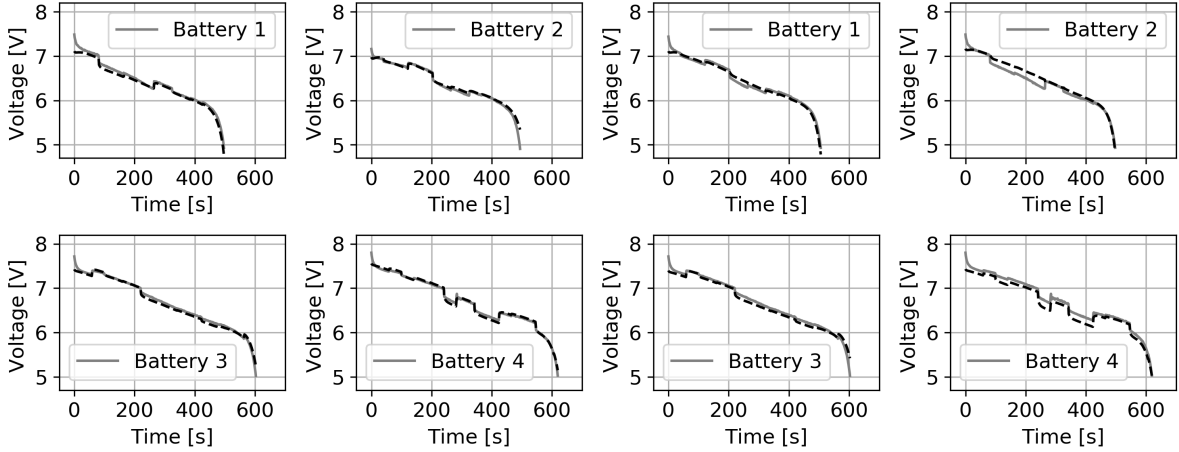


Figure 5. Prediction of discharge curves under variable loading conditions during the early stages of battery life for two batteries cycled within a load level of 16 - 19 A (top row) and a load level of 12.9 A - 16 A (bottom row).

where the x-axis represents total cycle time in hours. The top row shows the discharge currents, whereas the bottom row shows the corresponding voltage discharge curves. Early in the battery life, the prediction aligns closely to the actual discharge curve, which suggests proper initial training of the aging parameters (q^{max} , R_b), as well as for the non-ideal voltage MLP. As batteries age, the prediction deviates from the ground truth. This suggests that the aging parameters q^{max} , which mainly influences the rate of discharge for the same current level, and R_b , which mainly influences the voltage drop on the linear discharge portion, deviate from their early-life values due to battery degradation. On the other hand, the staircase-like behavior of the voltage curve during discharge is captured fairly well also in later stages, which suggests a correct prediction of the non-ideal voltage throughout the battery life. We conclude the non-ideal voltage MLP weights can remain fixed after training on early life data and used for predictions later in life. To capture aging effects, the focus is hereby directed to the parameters q^{max} and R_b .

5.2. Load Level-Dependent Aging Model

In order to accurately predict voltage discharge curves of aged batteries, it is necessary to learn the aging parameters at different stages of life¹. Since the batteries are subject to a wide range of different load levels, which drives large variation in temperature build-up and Li-ion concentration gradients, we identified the discharge current level as one of the main factors that drives cell aging. To determine q^{max} and R_b as function of age in form of cumulative energy and loading conditions in form of discharge current, the parameter pair is updated using constant-current discharges picked at regular intervals from the training dataset. In Fig. 7 one can

see the decrease of q^{max} over cumulative energy for each of the five different load levels, highly correlated with battery capacity determined through reference discharges at the same age levels than the q^{max} values. We chose to show the q^{max} and capacity values in 20 cycle intervals until reaching 100 missions and in 100 cycle intervals thereafter, in order to achieve greater clarity and readability of the q^{max} and capacity relation.

One of the main observations from this plot is the dependency of the aging rate on the load level, where high current leads to more aggressive aging and earlier cell failure. As it can be clearly seen, the cell failure at 19 A occurs at 2.15 Ah capacity, whereas at 9.3 A the battery end of life is reached at approximately 1.8 Ah capacity. The aging trend between capacity and q^{max} closely aligns and, therefore, q^{max} can be expressed as function of capacity where only a multiplying factor is needed for conversion. Parameter R_b shows a similar aging trend to q^{max} , as expected, due to internal aging mechanisms increasing throughout the aging process.

Once q^{max} and R_b are identified at regular intervals over the lifetime, the model can be updated and predict EOD at different aging levels. As we show in Figure 8, where we compare model predictions with outdated (early-life) and updated model parameters, this is a fundamental step for accurate EOD predictions. It can also be corroborated by the results in Fig. 6 where, by using outdated aging parameters, the model struggles to predict both the portion of the discharge curve that follows a linear trend and the non-linear final discharge portion, which results in a larger EOD prediction error. Updating the aging parameters helps the model to predict the discharge curve more accurately with minor deviations at larger load level steps. Especially, the non-linear voltage drop right before EOD is captured more accurately with updated model parameters.

¹It should be remembered that this is a phenomenological-based, approximate representation of the aging mechanisms

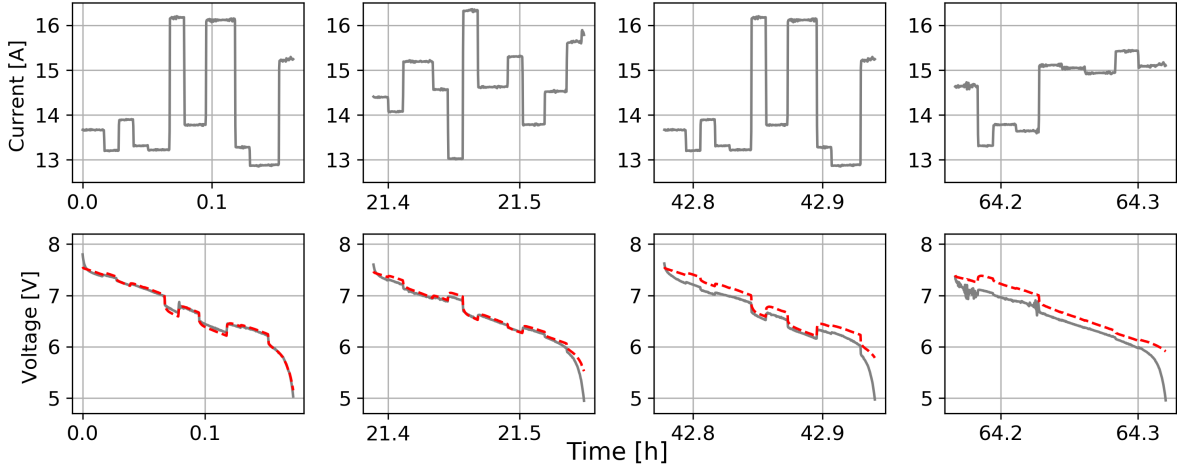


Figure 6. Prediction of discharge curves under variable load at different stages of battery life, from left to right, where the model aging parameters q^{max} and R_b are kept frozen to the original values learned during the first discharge cycles, showing how these parameters affect the model error later in life.

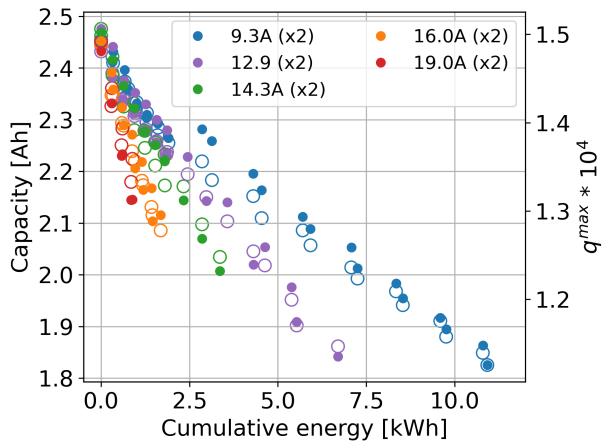


Figure 7. Degradation of battery capacity (solid dots, left y-axis) and q^{max} (circles, right y-axis) as function of cumulative energy for constant current loading.

5.3. Aging Parameter Updating with Gaussian Process Regression

With the goal of forecasting discharge curves outside of the training dataset, we chose a Gaussian process regression implemented using the GPyTorch package to build a model that can be used for interpolation and extrapolation while also providing confidence intervals for uncertainty quantification. Figure 9 illustrates the Gaussian process model for q^{max} and R_b on the left and right plots, respectively. The circles are the data points at different load levels, while the solid lines and corresponding shaded areas represent the GP mean and 95% confidence intervals.

In order to minimize the effect of aleatoric uncertainty, the

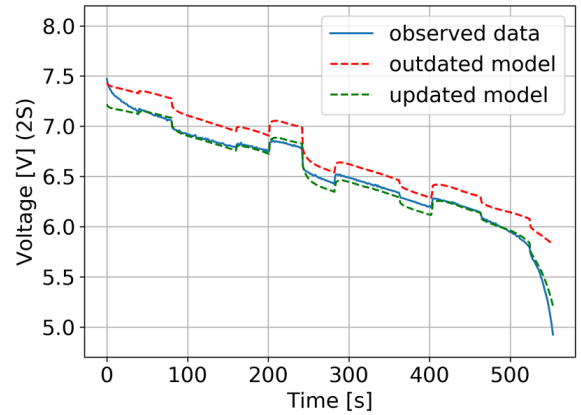


Figure 8. Discharge curve prediction with outdated and updated aging parameters for a 1kWh aged battery.

data was normalized through dividing each data point by the initial value at 0 kWh for each load level. Since this dataset is intended to focus on load level variations, the battery-to-battery variation is difficult to capture due to different aging curves over life time, since only two batteries were aged at each level. Nevertheless, at the very beginning of the battery life cycle process (at or close to 0 kWh) the effect of different load levels on the aging parameters is negligible.

Advancing further into the battery life, different load levels take the predominant role with regards to variation in battery aging, where the GP model captures the load level variation as function of age while providing enough flexibility to smooth out outlier values.

Both GP models for q^{max} and R_b are built with linear mean functions to capture the linear trend that can be seen for each

load level after a sharper initial drop of the parameter values. Aligned with our expectations, the sharper increase of R_b on more aggressive load levels compared to milder current levels is clearly visible. In the next step, the GP model is validated on unseen data. For this purpose we perform a cross-validation study by excluding one load level from the training dataset and using it as a test case.

Figure 10 shows an excerpt of the performed cross-validation study, where the top row shows constant current prediction results on 9.3 A, the middle row constant current prediction on 12.9 A, and the bottom row shows variable current prediction results for a load level with range 12.9 A - 16 A. The two leftmost columns show prediction results without any early life data of the predicted load level, whereas the two rightmost columns use updates with early life data, where the full circles are included and empty circles excluded from the training data. The data points included in the model training are plotted using a gray-scale.

The constant-current prediction on 9.3 A without early life data shows some significant deviation from the ground truth. The prediction performed until 11 kWh is far outside the cumulative energy range of data included in the training set, which is bounded at 7 kWh through the closest load level at 12.9 A. Updating the model with early life data until 6 kWh significantly improves the prediction results for both q^{max} and R_b . The mean of the GP model adheres more closely to the 9.3 A data points and the 95% confidence intervals shrink significantly even for prediction.

On the other hand, as shown in the second row, constant current level predictions on data within the bounds of the training dataset yield quite precise results, even in the case without including early life data, as the GP model does a fairly good job of matching the q^{max} values of the entirely excluded load level of 12.9 A. A slightly larger deviation can be seen for the R_b prediction, where later in life (3 kWh and older) the model shows a minor over-prediction. Adding early life data until 3 kWh to the model training gives a visible improvement, especially by narrowing the 95 % confidence interval for q^{max} close to the actual EOL and considerably improving the mean prediction of R_b .

The cross-validation study for the variable load cases with current limits between 12.9 A - 16 A shows similar results, as the variable load level remains within the bounds of the included training data. Both cases, with and without early life data, show close alignment with the ground truth data for both parameters, q^{max} and R_b . Since the prediction for this load level shows already good results, the inclusion of early life data for the aging parameters until 3 kWh does not show major improvements.

From these results, it can be concluded that predictions far outside the included training data require an early life update

in order to align with the ground truth data, but predictions performed within the bounds of the training data achieve good results even without including early-life data points.

5.4. Discharge Curve Forecast using Aging Parameter Model

We performed discharge predictions on aged batteries using the predicted aging parameters from the GP models with and without early life data. Figure 11 shows the prediction of the voltage discharge curve at different aging levels under both constant and variable loading. Constant-current prediction results are shown for 9.3 A and 12.9 A on the top two rows, and for 12.9 A - 16 A random loading conditions on the bottom row. The predictions are performed at 4, 6 and 8 kWh for the 9.3 A case and 3, 4 and 5 kWh for the remaining two cases, where the model aging parameters q^{max} and R_b used for the voltage prediction are themselves predicted from the Gaussian process model at the same age level, shown in Fig. 10. On the one hand, only observed predictions from cross validation interpolations are used and on the other hand prior information, where the q^{max} and R_b values until a certain age level (e.g. 1 kWh), are used for predictions at a later stages of life. The predictions for the 9.3 A discharge curves without early life data (blue curves) deviate from the measurements at all 3 predictions at 4 kWh, 6 kWh and 8 kWh. Here, the q^{max} values are over-estimated, e.g. 0.94 compared to actual 0.9 at 4 kWh, and the R_b values under-estimated, e.g. 1.37 to actual 1.51 at 4 kWh. Performing predictions with aging parameters using early life data until 3 kWh improve prediction results significantly (orange curve).

All predictions for the 12.9 A discharge case follow the linear discharge portion closely and predict the non-linear portion shortly before reaching the cut-off voltage at 5.0 V, close to satisfy an end-of-discharge prediction within an 1 % window. Here both cases, with and without early life data used for the aging parameter predictions, yield good prediction results when compared to the ground truth discharge curves.

Similar prediction results can be observed in the variable loading discharge case where at 3 kWh, 4 kWh and 5 kWh the model prediction with and without early life aging parameter information follow the discharge curves closely. The voltage prediction shows minor deviation from the staircase-like discharge behavior but the EOD prediction is also within an 1 % window for all cases. Also in the variable loading case, the improvement achieved through adding early life data to the aging parameter predictions is marginal.

A general observation holding for all prediction cases is that predictions farther ahead in the battery life show larger discrepancies than in early life. We speculate the latter to be caused by training the MLPs with early-stage life data, and the model might need further refinement to fully capture the aging behavior beyond the parameters (q^{max} , R_b) we chose.

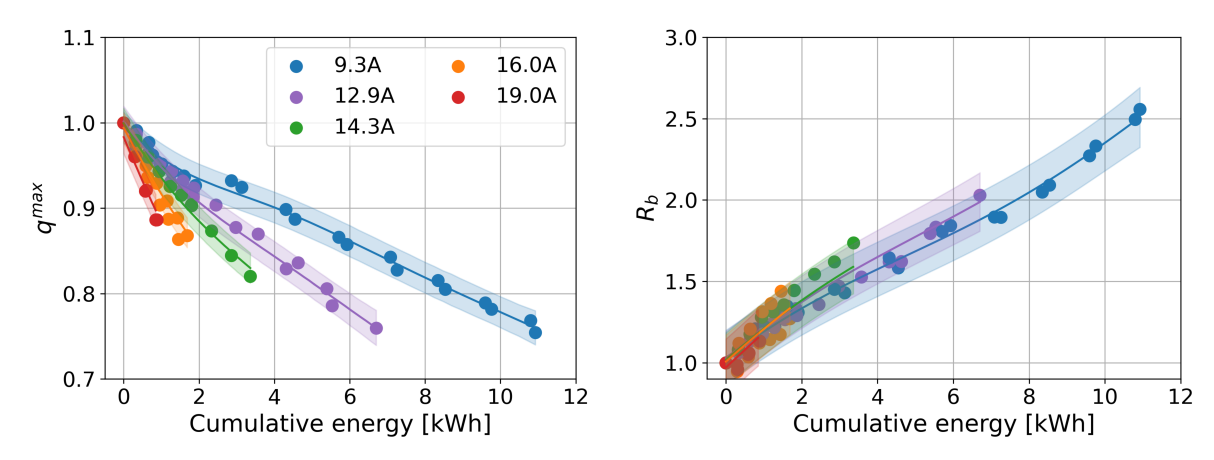


Figure 9. Gaussian process regression model for q^{max} and R_b as function of loading conditions and cumulative energy. Both quantities are normalized with respect to their initial estimates.

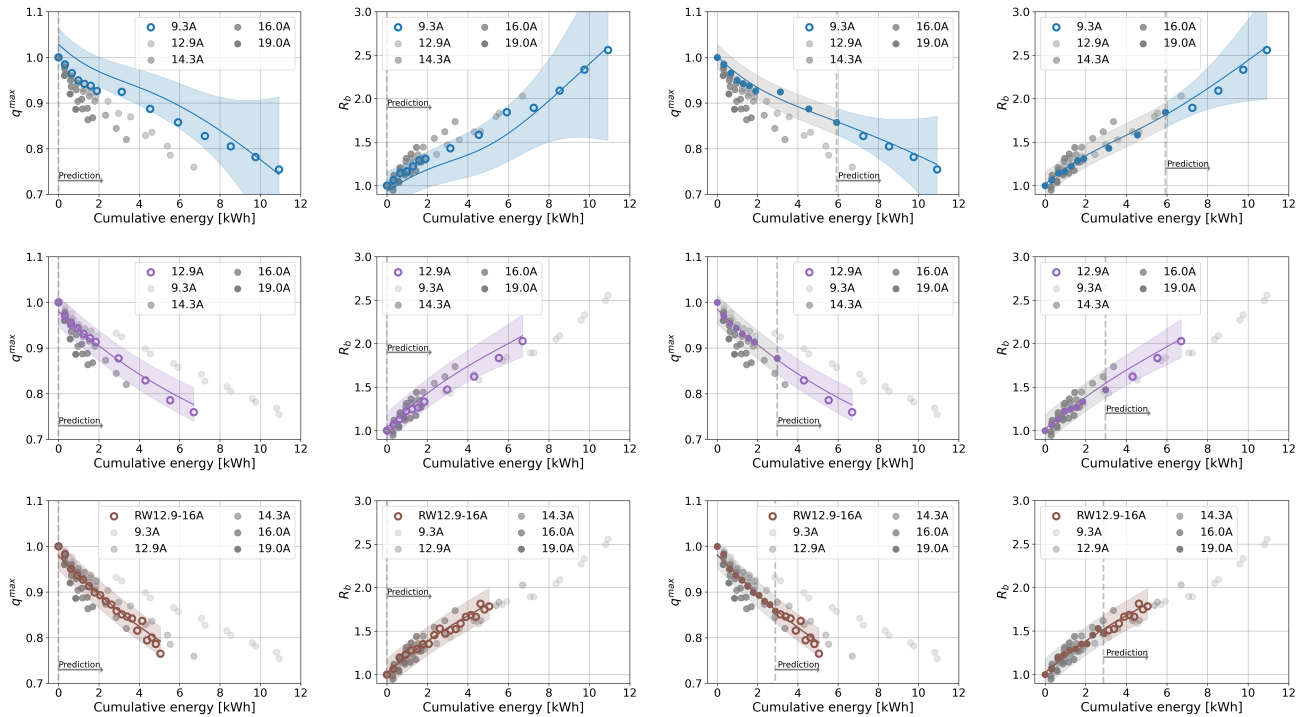


Figure 10. Forecast of q^{max} and R_b as function of cumulative energy for constant current at 9.3 A (top panels) and 12.9 A (middle panels) and variable current at 12.9 A - 16 A (bottom panels). Predictions are done without (two left-most columns) and with (two right-most columns) updates of q^{max} , R_b with early life data. The solid curves represent the mean function and the shaded areas cover the 95% confidence intervals.

Therefore, minor non-linearities might not be captured.

5.5. Discussion on Assumptions and Drawbacks

Our approach in this paper is based on the assumption that data from a fleet of batteries subjected to a wide level of discharge currents is available and their capacity as well as aging parameters were estimated at regular intervals. Without a fleet-wide aging parameter characterization or with a narrow operating window, the prediction uncertainties would increase for batteries outside of the observed operating range.

We want to address the model sensitivity decrease when approaching the outer limits of the load range batteries were subjected to in this research. Discharge predictions for variable load cases from 16 - 19 A that reach the maximum current used in this dataset show precision loss in terms of tracking the staircase-like voltage behavior, especially later in the battery life. This drawback can be an artifact of the non-ideal voltage MLP training that, in order to capture the outer limits of the dataset, might require more data points covering corner cases.

Lastly, we want to point out that the model discharge predictions in the first few seconds after the load is applied show some deviation from the actual data. Here, the non-linear initial voltage drop grows with larger applied currents and shows also more distinct drops later in life. While the model can cover some of the initial non-linearities for lower load levels and especially for predictions at early life stages, forecasts on higher load levels, especially performed on aged batteries, show a significant deviation in the first seconds of discharge. This issue can possibly be addressed through a more complex architecture for the non-ideal voltage MLP, or by adaptations to the electrochemistry-based model equations.

6. SUMMARY AND CLOSING REMARKS

In this paper we presented an enhanced hybrid physics-informed machine learning model for discharge and aging prediction on a battery fleet covering a wide range of load levels. We based our approach on a reduced-order electrochemistry discharge model that was previously introduced in combination with a data-driven machine learning kernel to predict voltage curves during discharge, and further improved this approach by accounting for the effects of a large variety of applied current levels and temperature build-up during discharge cycles.

Furthermore, we built a Gaussian process model to predict the battery aging parameters q^{max} and R_b as function of cumulative energy and discharge current levels. The model uses data from a fleet of similar batteries subjected to different load levels to predict aging parameters without the need to perform parameter identification via reference discharge cycles at regular intervals.

The proposed hybrid discharge model aims at improving discharge predictions for battery fleets subjected to a large variety

of mission profiles. The GP aging model helps to further improve predictions of discharge curves further ahead in the battery life, by using aging parameter estimates from a fleet of similar batteries subjected to different loading profiles. The laboratory-generated dataset helped us train and validate the models using simplified, yet representative, variable loading profiles. Future work will comprise further model design optimization, with the intent to capture initial non-linear voltage drop and discharge curves from loading conditions close to the boundaries of the available dataset.

ACKNOWLEDGMENT

The work of Matteo Corbetta and Chetan Kulkarni was supported by the System-Wide Safety (SWS) project under the Airspace Operations and Safety Program within the NASA Aeronautics Research Mission Directorate (ARMD).

A. REDUCED-ORDER MODEL

The reduced-order, electrochemistry-based model developed in (Daigle & Kulkarni, 2013) is based on the high-fidelity model presented in (Karthikeyan, Sikha, & White, 2008). In this appendix a brief summary of the model is provided. The overall output voltage is estimated by:

$$V = V_{U,p} - V_{U,n} - V_0 - V_{\eta,p} - V_{\eta,n},$$

The equilibrium potential on the positive and negative electrode V_U is based on the Nernst equation:

$$V_{U,i} = U_0 + \frac{RT}{mF} \ln \frac{1 - x_i}{x_i} + V_{ni,i},$$

where the electrode (negative or positive) is indicated by the subscript $i = \{n, p\}$; U_0 is the reference potential; R is the universal gas constant; T is the electrode temperature; m is the number of electrons transferred in the reaction; F is the Faraday constant; x is the mole fraction for the Lithium-intercalated host material; and $V_{ni,i}$ is what has been defined in (Daigle & Kulkarni, 2013) as ‘‘internal’’ voltage, an activity correction term null in ideal conditions. Details about V_{ni} will be provided hereafter.

The mole fraction represents the ratio between the number of ions in each electrode and the maximum number of available ions in both electrodes combined:

$$x_i = q_i / q^{max}, \quad \text{and} \quad q^{max} = q_n + q_p.$$

As there is a Li-ion concentration gradient between the surface and the bulk of each electrode, which is amplified with larger loading conditions a Li-ion diffusion rate is defined:

$$\dot{q}_{bs,i} = \frac{1}{D} (c_{b,i} - c_{s,i}),$$

where D is the diffusion parameter and subscripts refer to bulk

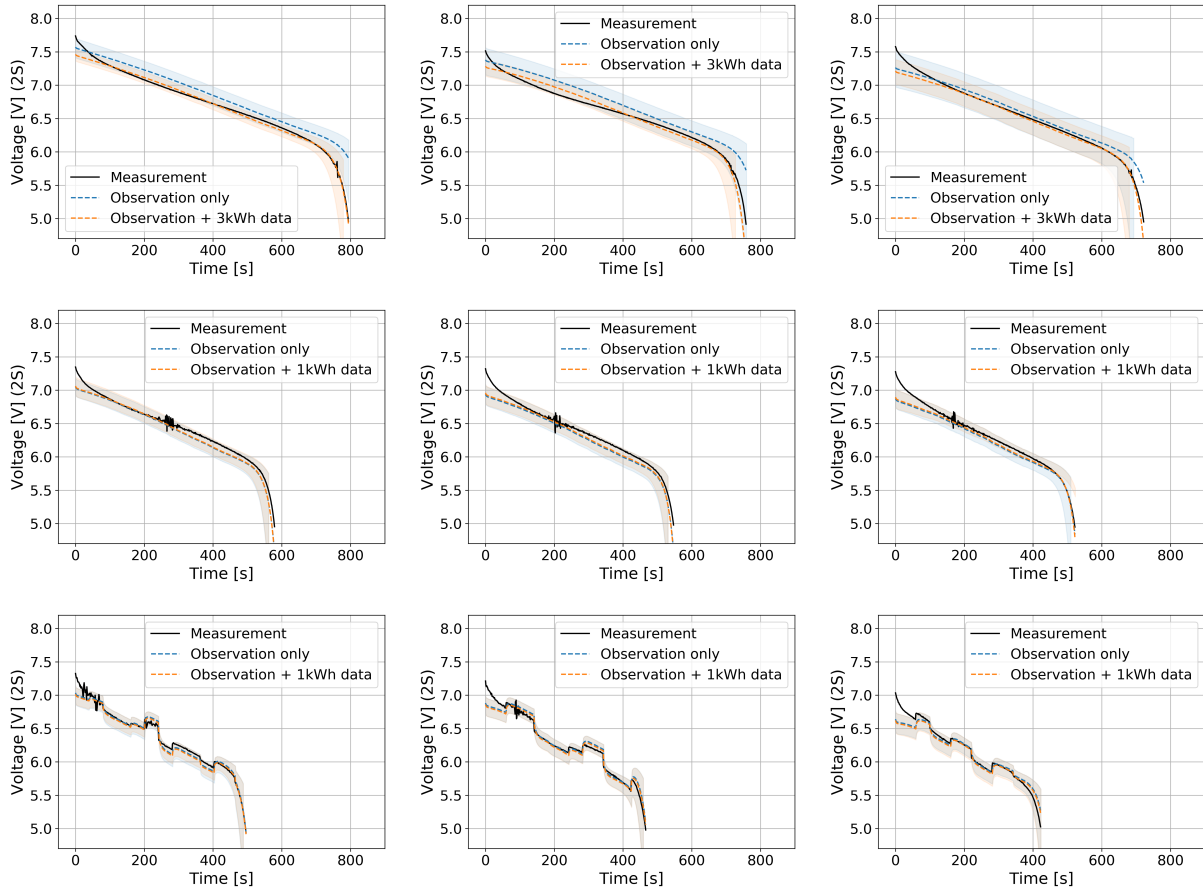


Figure 11. Forecast of voltage discharge curves for constant 9.3 A (top row) and 12.9 A (middle row) and variable loading conditions 12.9 A - 16 A (bottom row). From left to right, the predictions are done at 4 kWh, 6 kWh and 8 kWh (9.3A) as well as 3 kWh, 4 kWh and 5 kWh (12.9 A and 12.9 A - 16 A). Each prediction uses forecasts of q^{max} and R_b values from fleet observations only or including early life data until 3 kWh (9.3 A) and 1kWh (12.9 A and 12.9 A - 16 A). The solid line represents the prediction mean and the shaded areas cover the 95% confidence intervals.

b , surface s , and negative or positive electrode i , respectively. The diffusion parameter is significantly influenced by the cell temperature, which we address by applying the Arrhenius' law:

$$D = D_b \cdot e^{D_\tau \left(\frac{1}{T} - \frac{1}{T_{ref}} \right)},$$

where D_b is the base diffusion rate at ambient temperature, D_τ the diffusion parameter handling the influence of temperature, T represents the cell temperature and T_{ref} the reference temperature, commonly defined as 293 K. Differently from R_0 , we fix the parameters D_b and D_τ based on early-life discharge cycles and do not model them as a function of cumulative energy drawn (i.e., aging effects on D are neglected).

The baseline electrochemistry model estimates the non-ideal voltage through the Redlich-Kister expansion (Karthikeyan et al., 2008):

$$V_{INT,i}(x_i; \mathbf{A}_i) = \frac{1}{mF} \sum_{k=0}^{N_i} A_{k,i} \left((2x_i - 1)^{k+1} - \frac{2x_i k (1 - x_i)}{(2x_i - 1)^{1-k}} \right).$$

The mole fraction x_i represents the input to the non-ideal voltage estimation, whereas the coefficients $A_{k,i}$ are identified through data-fitting, and the number of elements in the sum N_i is empirically-derived. This polynomial expansion is substituted by the MLPs in the proposed hybrid model, as discussed in this paper and in (Nascimento et al., 2021a, 2021b).

The solid-phase Ohmic resistance, electrolyte Ohmic resistance, and current collector resistance can be lumped together into R_0 to calculate the voltage drop: $V_0 = i_{app} R_0$, where i_{app} is the discharge current. Here, we also use Arrhenius' law for the estimation of R_0 as function of cell temperature as described in 4.

REFERENCES

- Bole, B., Kulkarni, C., & Daigle, M. (2014). Randomized battery usage data set. *NASA AMES prognostics data repository*, 70.
- Daigle, M. J., & Kulkarni, C. S. (2013, Sep). Electrochemistry-based battery modeling for prognostics. In *2013 annual conference of the phm society* (p. 13 pages). New Orleans, USA: PHM Society.
- Dubarry, M., Truchot, C., & Liaw, B. Y. (2012). Synthesize battery degradation modes via a diagnostic and prognostic model. *Journal of Power Sources*, 219, 204--216.
- Gardner, J. R., Pleiss, G., Bindel, D., Weinberger, K. Q., & Wilson, A. G. (2018). Gpytorch: Blackbox matrix gaussian process inference with gpu acceleration. In *Advances in neural information processing systems*. Introduction of inr18650-25r [Computer software manual]. (2013, 10).
- Karthikeyan, D. K., Sikha, G., & White, R. E. (2008). Thermodynamic model development for lithium intercalation electrodes. *Journal of Power Sources*, 185(2), 1398--1407.
- Lutsey, N., & Nicholas, M. (2019). Update on electric vehicle costs in the united states through 2030. *Int. Counc. Clean Transp*, 12.
- Lyu, Z., Wang, G., & Gao, R. (2021). Li-ion battery prognostic and health management through an indirect hybrid model. *Journal of Energy Storage*, 42, 102990.
- Nascimento, R. G., Corbetta, M., Kulkarni, C. S., & Viana, F. A. C. (2021a). Hybrid physics-informed neural networks for lithium-ion battery modeling and prognosis. *Journal of Power Sources*, 230526. doi: 10.1016/j.jpowsour.2021.230526
- Nascimento, R. G., Corbetta, M., Kulkarni, C. S., & Viana, F. A. C. (2021b, Nov-Dec). Li-ion battery aging with hybrid physics-informed neural networks and fleet-wide data. In *2020 Annual Conference of the PHM Society*. Virtual Event: PHM Society. Retrieved from <https://doi.org/10.36001/phmconf.2021.v13i1.2998> doi: 10.36001/phmconf.2021.v13i1.2998
- Nascimento, R. G., Fricke, K., & Viana, F. A. C. (2020). A tutorial on solving ordinary differential equations using Python and hybrid physics-informed neural networks. *Engineering Applications of Artificial Intelligence*, 96, 103996.
- Paszke, A., Gross, S., Massa, F., Lerer, A., Bradbury, J., Chanan, G., ... Chintala, S. (2019). Pytorch: An imperative style, high-performance deep learning library. In *Advances in neural information processing systems* 32 (pp. 8024--8035). Curran Associates, Inc. Retrieved from <http://papers.neurips.cc/paper/9015-pytorch-an-imperative-style-high-performance-deep-learning-library.pdf>
- Tampier Cotoras, C., Perez, A., Jaramillo Montoya, F., Quintero, V., Orchard, M., & Silva, J. (2015, 10). Lithium-ion battery end-of-discharge time estimation and prognosis based on bayesian algorithms and outer feedback correction loops: A comparative analysis..
- Zhang, Y., Xiong, R., He, H., & Liu, Z. (2017). A lstm-rnn method for the lithium-ion battery remaining useful life prediction. In *2017 prognostics and system health management conference (phm-harbin)* (pp. 1--4).